Study of the Mechanism of the N−CO Photodissociation in *N*,*N*-Dimethylformamide by Direct Trajectory Surface Hopping Simulations†

Mirjana Eckert-Maksić* and Ivana Antol

Rudjer Bošković Institute, Division of Organic Chemistry and Biochemistry, POB 180, HR-10002 Zagreb, Croatia

Received: May 18, 2009; Revised Manuscript Received: June 15, 2009

Photodynamics of *N*,*N*-dimethylformamide (**DMF**) in its low-lying singlet excited $n_O-\pi^*$ and $\pi-\pi^*$ states have been explored by the direct trajectory surface hopping method based on multiconfigurational ab initio calculations. The dynamics simulations starting in the first excited singlet state ($n_O-\pi^*$) showed that in 57% of trajectories, S_1 excited **DMF** decays to the ground via the crossing seam related to the N−CO bond stretching **MXS1**. In 41% of all trajectories, the relaxation process on the S_1 PES moves the molecule into the minimum, where it stays trapped until the end of simulation time. In simulations starting in the second excited state, all trajectories are found to deactivate through **MXS5** (S_2/S_1) by very fast N−CO stretching. Because the N−CO dissociation process continues in the S_1 potential energy surface, most of the population overshoots the **MXS1** and leads to fully dissociated electronically excited HCO and $N(CH_3)_2$ radicals. A mechanism for their deactivation by H−C−O and C−N−C bending modes is proposed.

Introduction

Knowledge of how the peptide bond interacts with ultraviolet light is of crucial importance for understanding the effect of light irradiation on various life forms. In addition, it also has significant implications in many other fields such as modern structural biology, laser surgery, or photodegradation of industrially important polymeric materials.[2] In this vein, investigation of the photochemistry of the peptide model compounds has received much attention from both experimental[3−9] and theoretical points of view.[10−13] Most of these studies have been focused on formamide, which is the simplest prototype of the peptide bond. Photodissociation of formamide has been studied experimentally in solution,[14] in the gas phase,[15] and in argon and xenon matrices,[4] as well as computationally.[4,10] Recently, we have also studied dynamics of the photodissociation processes of formamide[16] and its O- and N-protonated forms[17] by employing the mixed quantum-classical direct trajectory method with surface hopping at the state average complete active space self-consistent field CASSCF(10,8)/6-31G(d) level. The calculation for formamide confirmed that N−CO dissociation is the major process from the first and the second excited states. Protonation was found to influence both the mode of dissociation as well as its time scale. Therefore, in the first excited state of O-protonated species, two deactivation processes were found: the C−N (major) and the C−O (minor) dissociations with very short lifetime, whereas the second excited state underwent C−O dissociation with the lifetime of only 11 fs. The major process for decomposition in the first excited state of N-protonated formamide involved C−N dissociation with a lifetime of 390 fs; however, 55% of trajectories remained undeactivated.

Investigations of photodissociation of **DMF** have attracted much less attention. The only gas-phase experimental study was published by Butler and coworkers some 10 years ago.[7,8] By measuring the photofragment velocity and angular distribution of DMF at 193 nm excitation in the second excited singlet state (π,π^*), they found that the C−N bond cleavage proceeded either along the excited state pathway leading to $HCO(\tilde{X}^2A')$ + $N(CH_3)_2(\tilde{A}\ ^2A_1)$ (eq 1) products or through decay channel resulting in $HCO(\tilde{X}^2A')$ + $N(CH_3)_2(\tilde{X}^2B_1)$ (eq 2) fragments in the ground state. They also found evidence of the cleavage of the N−CH_3 bond leading to the formation of $HCONCH_3$ + CH_3 (eq 3)

$$HCON(CH_3)_2 + 193\ nm \rightarrow HCO(\tilde{X}^2A') + N(CH_3)_2(\tilde{A}^2A_1) \quad (slow) \quad (1)$$

$$\rightarrow HCO(\tilde{X}^2A') + N(CH_3)_2(\tilde{X}^2B_1) \quad (fast) \quad (2)$$

$$\rightarrow HCONCH_3 + CH_3 \quad (3)$$

The C−H bond dissociation channel, which could also be envisaged as a potential dissociation path, was not observed in this experiment. The relative yields for channels 1−3 were determined to be (0.49 ± 0.09):(0.15 ± 0.04):(0.36 ± 0.07).

Subsequently, Fang and coworkers[11] carried out complete active space self-consistent field (CASSCF) calculations for the above proposed photodissociation paths in the first excited singlet n_O,π^* and triplet states. On the basis of the obtained results, they concluded that most of the N−CO cleavage takes place at the S_1 surface and partially at the T_1 surface. They also found evidence of the formation of $HCONCH_3$ and CH_3 from the T_1 surface. It is also important to mention that they excluded the possibility of forming products from the S_2 state, which according to Butler's work[7,8] was responsible for the formation of the ground-state HCO radical and the excited-state $N(CH_3)_2$ radical. Namely, they claimed that the molecule, upon excitation of 193 nm, which was employed experimentally, could not reach the S_2 state but instead resulted in molecules in the excited

† Part of the "Russell Pitzer Festschrift".

* Corresponding author. Fax: (+)385-1-4680-195. E-mail: mmaksic@emma.irb.hr.

10.1021/jp9046177 CCC: $40.75
Published on Web 07/15/2009

vibrational states of the S_1 electronic state. However, because of the vibronic coupling between the S_2 and the S_1 electronic state, some of the molecules in the highly excited vibrational state of the S_1 electronic state dissociate into ground-state HCO and the excited-state $N(CH_3)_2$ fragments along the S_2 pathway, whereas the rest of them relax toward the S_1 minimum.

In the present work, we address photodissociation of **DMF** by means of the same computational approach, which was used in our previous studies on the photodissociation of formamide and its protonated forms.[16,17] Our main aim in undertaking this work was to provide deeper insight into the mechanism and dynamics of photodissociation of the N−CO bond in **DMF** in the n_O,π^* (S_1) and the π,π^* (S_2) excited singlet states. Given that in the experimental setup, the 193 nm light was used (with excitation energy of 6.42 eV) and experimental absorption maximum for the π,π^* state appears at 197.4 nm (6.28 eV), involvement of the S_2 state in considering the photodissociation processes is, in our opinion, fully justified. The special emphasis in discussing results will be put on assessing the impact of substitution of the N terminal of the peptide moiety by the methyl groups on the mechanism of photodisociation of the bond connecting C═O and $N(R)_2$ (R═H, CH_3) chromophores. In what follows, we shall denote this type of dissociation as the N−CO dissociation to differentiate it from the cleavage of the methyl group from the nitrogen atom, which will be denoted as $N-CH_3$. In analogy to previous dynamic simulations of formamide and its protonated forms, Rydberg states were not taken into account.

Computational Details

For characterization of the potential energy surface (PES) of **DMF** as well as the dynamic simulations, state-averaged complete active space self-consistent field (SA-CASSCF) method was employed. The active space comprised ten electrons in eight orbitals (two σ/σ^* pairs, two nonbonding lone pairs, and one π/π^* pair of orbitals). This active space was found to be a good compromise for adequate characterization of the low-lying valence states and photodissociation processes in our previous studies on formamide. Three lowest singlet states with equal weights (SA-3) were included in the state average procedure. In addition, some of the critical points were also optimized with multireference configuration interaction method with singles and doubles (MRCISD), and their energies were further improved by inclusion of the Davidson correction (MR-CISD+Q). In these calculations, we constructed the total configuration state function (CSF) space by applying single and double excitations from all internal (active and double occupied) orbitals into all virtual orbitals for all reference CSFs. The final expansion space in the MRCISD calculations in terms of CSFs comprised the configurations obtained from a CAS(8,6) reference space. The five 1s core orbitals were kept frozen. The stationary points and the minima on the crossing seam (MXS) were calculated using analytic gradients and nonadiabatic coupling vectors computed as previously described.[19−23] Additional calculations were performed for CHO and for $N(CH_3)_2$ radicals at the SA-2-CASSCF(5,4)/6-31G(d) and CASSCF(7,6)/6-31G(d) levels, respectively. In the case of the HCO radical, active orbitals 6a′, 7a′, 1a″, and 2a″ (in C_s symmetry frame) were employed. Active orbitals for $H(CH_3)_2$ radical were $5a_1$, $6a_1$, $7a_1$, $4b_2$, $5b_2$, and $^2B_1$ (in C_{2v} symmetry frame). The H−C−O and N−C−N bending reaction coordinates were calculated following the minimum energy path in the ground as well as in the first excited state.

Simulations of photodissociation dynamics were carried out using the direct trajectory surface hopping method. A full description of the methods used in dynamics simulations has been described in detail in a number of recent papers by Barbatti and Lischka[24] and in our previous studies on formamide[16] and its protonated forms.[17] Nonadiabatic transition probabilities between electronic states were obtained on the basis of the improved version of the fewest switches algorithm[25] proposed by Hammes-Schiffer and Tully.[26] The nuclear motion was represented by classical trajectories computed by numerical integration of Newton's equations using the velocity Verlet algorithm[27] with a step size of 0.25 fs. The maximal time for trajectory runs from the S_1 and S_2 states was set to 1000 and 500 fs, respectively. The initial Cartesian coordinates and momenta were selected from a Wigner[28] distribution for the quantum harmonic oscillator at the ground electronic and vibrational states. No restriction on frequencies was employed. Two batches of 100 trajectories each were calculated starting in the S_1 ($n_O-\pi^*$) and S_2 ($\pi-\pi^*$) valence states, respectively. Geometry optimizations of the minima and the transition-state structures and MXS searches were performed with the COLUMBUS program system.[29] The atomic orbital (AO) integrals and AO gradient integrals have been computed with program modules taken from DALTON.[30] The ground-state equilibrium geometry and vibrational modes used in the initial condition generation in dynamics simulations were calculated by the density functional theory DFT(B3LYP)/SV(P)[31,32] method using the TURBOMOLE[33] program. The 6-31G(d) basis set[34] was used in all calculations. The dynamic simulations were carried out by means of the NEWTON-X program package[35] using the analytic gradients and nonadiabatic coupling vectors computed by COLUMBUS.

Results and Discussion

A. Critical Points and Reactions on the S_1 Potential Energy Surface. As mentioned earlier, the PES for dissociation of the **DMF** in the S_1 and S_2 states in the present work has been characterized by means of CASSCF(10,8) method. This method is well known to overestimate vertical excitation energies, in particular, those for the π,π^* states, because of the lack of major dynamical electron correlation. In the case of **DMF**, the calculated vertical excitation energies overshoot the experimentally[36,37] measured values for the n_O,π^* and π,π^* by ca. 0.4 and 1.8 eV, respectively, which is slightly more than those in the case of formamide. Similar, but somewhat less pronounced, deviation was also observed by comparison with the CASSCF/CASPT2 values published by Serrano-Andres.[38] Nevertheless, the changes of the calculated vertical excitation energies upon going from formamide to **DMF** closely follow the trend of changes in the measured values, that is, the first excitation energy remains practically constant, whereas the vertical excitation energy for the π,π^* (S_2) state decreases. Therefore, it is reasonable to expect that this will not influence the quality of our dynamical calculations more than in the case of formamide. Namely, as already emphasized in our previous study on formamide[16] and its protonated forms,[17] the employed method represents a satisfactory compromise between accuracy and computational efficiency, demanded by the on-the-fly dynamics simulations, where a full quantum chemical calculation has to be performed at every time step.[18] It should be stressed, however, that the prize to be paid due to overestimated S_2 excitation energy is a significant overshooting in the S_2 photodynamics. This problem has been discussed in more detail in refs 16 and 17.

Optimized equilibrium geometries, saddle points, and minima on the crossing seams are shown in Figure 1, whereas their

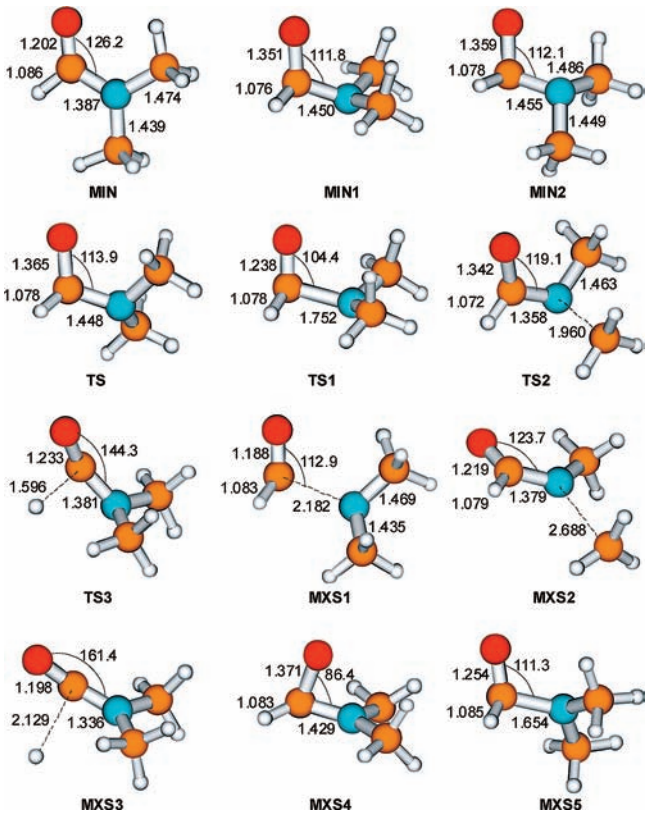

Figure 1. Key structural parameters of the structures of the stationary points in different electronic states of **DMF** at the CASSCF(10,8)/6-31G(d) level of theory. Distances are given in angstroms, and angles are given in degrees.

relative energies calculated relative to the ground-state minimum of **DMF** are given in Table 1 and Figure 2. Total electronic energies and Cartesian coordinates of all considered species are summarized in the Supporting Information.

Because the structural features of the calculated structures are not of focal interest here, we shall only briefly summarize some of their main characteristics. Their perusal shows that excitation to the S_1 state leads to pronounced pyramidalization at the carbon and nitrogen atoms and the lengthening of the central N−CO and C═O bonds, as expected for the peptide unit.[39] It is interesting to note that the length of the central N−CO bond is slightly longer, whereas the C═O bond length is shorter than that in formamide.[12] The other point worth noting is that the N−CO bond distances calculated in the present work are significantly different from those reported by Lee et al.,[11] whereas, the opposite holds for the C═O bonds. A similar trend is observed for the **TS1** structure in which the central N−CO bond is longer by ca. 0.14 Å relative to the CAS(14,10)/6-31G(2d,f) value. However, the length of the bonds that undergo dissociation in the **TS2** and **TS3** structures are much closer to those reported in ref 11. The comparison of the calculated MXS structures with those of their TS counterparts is also of interest. They are characterized by pronounced stretching of the dissociating bond relative to the corresponding TS structures. Another interesting feature concerns significant reduction of pyramidalization at the C and the N atoms of the peptide moiety in the **MXS1** and shortening of the C═O bond as compared with the **TS1**. The same trends were observed in the related structures of formamide. Finally, it is interesting to note that the geometry of **MXS4** resembles the structure of the $S_1/S_0(1)$ conical intersection found by Fang, which was claimed to have only a minor role in dissociation process.

The PES of **DMF** was previously studied by Fang and coworkers[11] at the CASSCF(14,11) and CASSCF(8,7) levels using 6-31+G(2d,f) basis set. At both computational levels, these authors found two energy minima for the S_1 structure corresponding to the *E* and the *Z* isomers, with the latter being 0.3(0.9) eV less stable. They also located three different transition structures for N−CO, N−CH_3, and H−CO bond dissociations as well as the S_1/S_0, corresponding to *Z* and *E* isomers, respectively. Surprisingly, we found that the **MIN1** is 0.04 eV (0.06 eV if the ZPVE correction is included) more stable than its *E* counterpart. Therefore, both structures were reoptimized at the MR-CISD level, and their energies were refined at the same level of theory by the inclusion of the quadruple correction (MRCISD+Q).[40] The ordering of the resulting relative energies (Table 1) in both cases was found to be identical to those obtained by the CASSCF method, thus providing additional support in favor of higher stability of the *Z* isomer (**MIN1**). The energy barrier for interconversion of the *Z* isomer at the CASSCF(10,8) level amounts to 3.9 kcal mol^{-1}, which is in excellent agreement with the barrier (3.8 kcal mol^{-1}) calculated for interconversion of the more stable S_1 minimum (in this case *E* isomer) to its less stable counterpart in ref 11. Irrespective of the above-mentioned disagreements, the calculated energetic ordering of the transition structures for the considered bond dissociation channels qualitatively follows that reported by Liu et al.[11] It is also important to note that in all cases energy barriers calculated in the present work are closer to the CASSCF(14,11) than to the CASSCF(8,7) values reported in ref 11. For instance, the energy barrier for the N−CO dissociation channel, which was found to be the energetically most favorable process, accounts for 0.27 eV (0.22 eV ZPVE corrected), as compared with 0.15 and 0.64 eV obtained by Liu et al.[11] using CASSCF(14,11) and CASSCF(8,7) methods, respectively. Finally, they are in good agreement with barriers calculated using MRCISD and MRCISD+Q methods (Table 1). All of these facts indicate that the CAS(10,8) level can be adequately used in the dynamics simulations.

In the vicinity of the saddle points for each of the considered dissociation channels in the S_1 state, a corresponding minimum on the crossing seam (MXS) was found. Their energy ordering was found to be similar to that in formamide[16] with one notable exception. Namely, in **DMF**, the global minimum on the crossing seem corresponds to the MXS related to the dissociation of the N−CH_3 bond (**MXS2**), whereas in formamide, the lowest MXS corresponds to the N−CO bond dissociation. However, although, the **MXS2** is the lowest energy MXS in **DMF**, it is not expected that it will get activated because the activation of conical intersection is regulated by the corresponding dissociation barrier, which is higher than the barrier for the cleavage of the central C−N bond by 0.69 eV (0.59 ZPVE corrected) (Table 1). The S_1/S_0 MXSs for the N−CO (**MXS1**), and the H−CO (**MXS3**) dissociation were found to be higher in energy than **MXS2** by 0.40 and 1.67 eV, respectively, thus following qualitatively the same trend as that observed in formamide. In contrast with the two lowest conical intersections, their energetic ordering closely follows the hierarchy of the corresponding saddle points (Figure 2, Table 1). In addition, similarly as in formamide, an additional MXS related to the OCN angle bending (**MXS4**) is located at 5.40 eV. It is also interesting to note that in contrast with formamide, all of the calculated MXSs possess energies below the vertical excitation energy of the S_1 (Figure 2).

Any attempt to optimize the second valence state of DMF failed because of the S_2/S_1 crossing in the vicinity of the

TABLE 1: Relative Energies (E_{rel}/electronvolts) and Description of Stationary Points in S_1 and S_2 Electronic States of DMF[a]

stationary point	MCSCF	MRCISD	MRCISD+Q	features
MIN[b]	0	0	0	ground-state minimum
S_1-vert	5.94	5.98	6.00	$n_O-\pi^*$ vertical excitation energy
S_2-vert	8.06	7.63	7.36	$\pi-\pi^*$ vertical excitation energy
MIN1	4.31(4.21)[c]	4.45	4.41	minimum in the S_1 excited state; *Z* isomer
MIN2	4.35(4.27)[c]	4.58	4.61	minimum in the S_1 excited state; *E* isomer
TS	4.48(4.38)[c]	4.70	4.72	saddle point for **MIN1** to **MIN2** isomerization by rotation around N−CO bond
TS1	4.58(4.43)[c]	4.59	4.55	saddle point for N−CO dissociation
TS2	5.27(5.02)[c]	5.53	5.45	saddle point for N−CH_3 dissociation
TS3	5.92(5.64)[c]			saddle point for H−CO dissociation
MXS1	4.13	4.31	4.36	S_1/S_0 MXS related to N−CO dissociation
MXS2	3.73			S_1/S_0 MXS related to N−CH_3 dissociation
MXS3	5.84			S_1/S_0 MXS related to H−CO dissociation
MXS4	5.40			S_1/S_0 MXS related to OCN bending
MXS5	5.39	5.27	5.20	S_2/S_1 MXS
MIN3	3.56	4.01	4.16	HCO (X^2A') + $N(CH_3)_2$ (X^2B_1) optimized with N−CO distance fixed to 10 Å
MXS6	4.78(1.31)[d]	5.26(1.25)[d]	5.41(1.25)[d]	MXS related to relaxation of HCO ($1^2A''$) radical
MIN4	5.30(1.74)[e]	5.59(1.58)[e]	5.70(1.54)[e]	$N(CH_3)_2$ (1^2A_1) minimum in the excited state
MXS7	5.52(1.96)[f]	5.81(1.80)[f]	5.93(1.77)[f]	MXS related to relaxation of $N(CH_3)_2$ (1^2A_1)

[a] MRCISD and MRCISD+Q values for some of the critical points are included for comparison. [b] Total electronic energies of the S_0 minimum are −247.05674, −247.64305, and −247.73550 au at the CASSSCF, MRCISD, and MRCISD+Q levels of theory, respectively. [c] ZPVE corrected values are given in parentheses. [d] Relative energy of linear HCO ($1^2A''/1^2A'$) with respect to the ground state HCO ($1^2A'$) is given in parentheses. [e] Relative energy of excited state $N(CH_3)_2$ (1^2A_1) with respect to the ground state $N(CH_3)_2$ (1^2B_1) is given in parentheses. [f] Relative energy of linear $N(CH_3)_2$ ($1^2A_1/1^2B_1$) with respect to the ground state $N(CH_3)_2$ (1^2B_1) is given in parentheses.

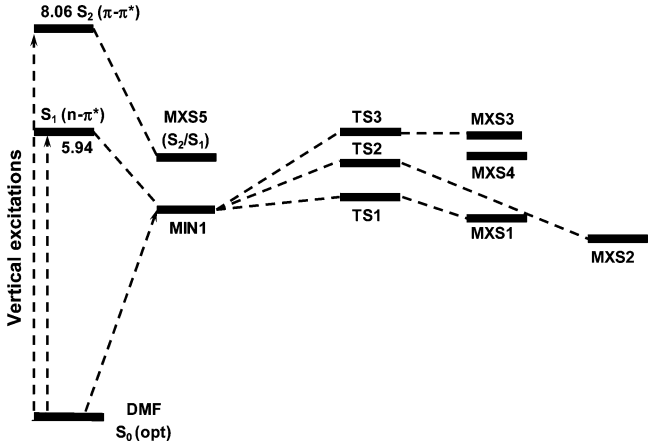

Figure 2. Energy scheme for **DMF** displaying vertical excitations, saddle points, and the MXSs.

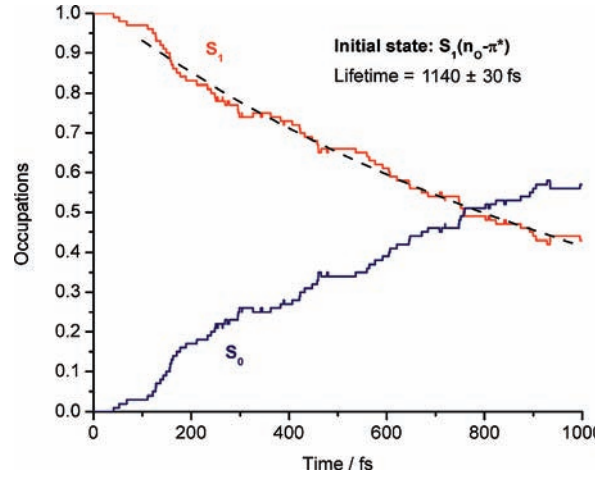

Figure 3. Fraction of trajectories for each state as a function of time after excitation of **DMF** into the S_1 initial state. The dashed line shows the exponential fitting curve.

Franck−Condon region. Likewise, in formamide, the relaxation starting from the Franck−Condon region is dominated by the stretching of the central N−CO bond, leading to the conical intersection between the S_2 and the S_1 states **MXS5** at 5.39 eV. Its structure (Figure 1) is characterized by the strongly elongated N−CO bond length (1.654 Å as compared with 1.387 Å in the Franck−Condon region, Figure 1); therefore, the relaxation to the S_1 state dominated by N−CO stretching may be expected.

The analysis given above suggests that replacement of the amino hydrogen atoms in formamide with the methyl groups should not have a pronounced effect on the N−CO photodissociation channel. There is only a difference in energy barrier for dissociation in the S_1 state, which is lower in **DMF** by 0.18 eV. Furthermore, the energy access in the FC point over the **TS1** structure in the two molecules is almost equal (1.36 eV in **DMF** vs 1.38 eV in formamide). Therefore, a similar mechanism of their photodissociation is expected. Despite that, the process differs considerably because in **DMF**, two paths differing in time scale are involved in photodissociation process (eqs 1 and 2), whereas in the case of formamide, only one pathway for cleavage of the N−CO bond was found both experimentally and computationally. To contribute to the better understanding of the differences in undergoing photodissociation mechanism in these two molecules, we have carried out dynamics simulations for the possible photodissociation paths in **DMF**. These results will be considered in the next sections.

B. Dynamics Simulations. Two sets of dynamic simulations were carried out starting from the n_O,π^* and the π,π^* states, respectively. The calculated fractional occupation in the S_1, S_2, and ground state as a function of simulation time is shown in Figures 3 and 4, respectively. The lifetime of each of the systems is calculated from a delayed exponential fitting with the function $f(t) = f_0 + \exp(-(t - \tau_d)/\tau_e)$, where $f(t)$ is the fraction of trajectories in the excited state and fitting parameters τ_d and τ_e represent initial delay and decay time constants, respectively. The lifetime for the excited states is then calculated as a sum of the τ_d and τ_e constants. Parameter f_0 denotes the fraction of trajectories that do not deactivate at all. The calculated lifetime of **DMF** in the S_1 excited states is found to be close to 1 ps,

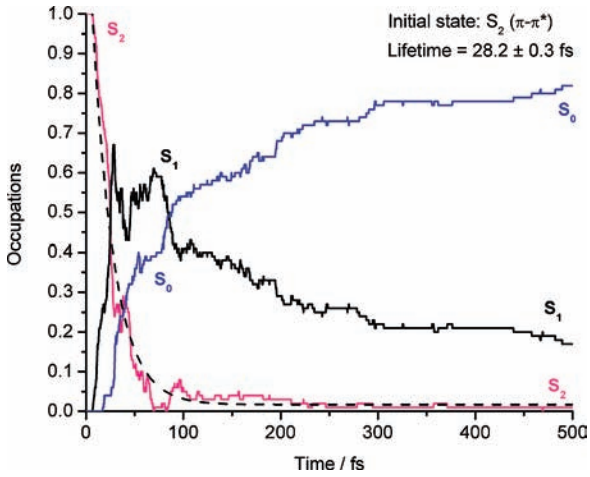

Figure 4. Fraction of trajectories for each state as a function of time after excitation of **DMF** into the S_2 initial states. The dashed line shows the exponential fitting curve.

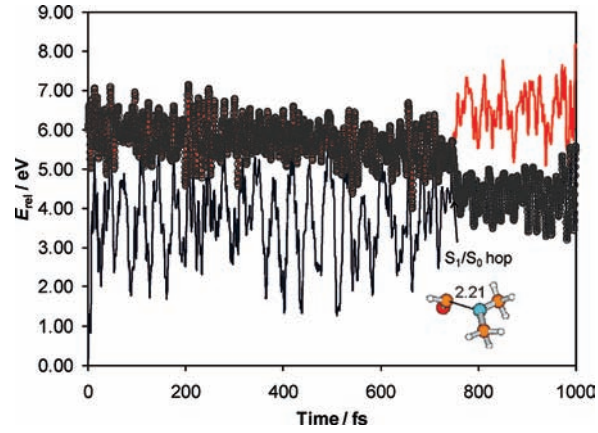

Figure 5. Time evolution of potential energies of the excited states and in the characteristic trajectory representing the N−CO stretching path with S_1 being the initial state. The dots in the potential energy graphs indicate the current state of the system.

which is considerably more than that in the case of formamide (Figure 3). Closer analysis indicates that this is mainly due to an interplay of an increase in a decay constant, τ_e, and reduction of f_0.

In contrast, the deactivation process of **DMF** after excitation to the S_2 (π,π^*) state proceeds much faster than that in formamide (Figure 4). The S_2 state starts to depopulate with a delay of only 6 fs and gets almost completely depopulated within 100 fs. The population of the S_1 and S_0 states increases to 50% around 50 and 90 fs, respectively. The overall estimated lifetime of **DMF** in the S_2 state is 28.2 ± 0.3 fs, as compared with 66 ± 1 fs found for formamide.[16] The reason for such a pronounced shortening of the lifetime for **DMF** can be traced back to the smaller mass-weighted distance between FC and S_2/S_1 MXS in **DMF** compared with that in formamide (3.75 amu$^{1/2}$ Å in **DMF** versus 3.88 amu$^{1/2}$ Å in formamide), which is mostly due to the extent of the N−CO bond stretching in passing from the FC region to S_2/S_1 MXS (0.27 Å in **DMF** vs 0.36 Å in formamide). In addition, difference in energy between the S_2/S_1 MXS and the calculated vertical excitation to the S_2 state in **DMF** is 0.3 eV smaller than that in the parent molecule.

C. Description of Typical Trajectories for Dissociation from the S_1 State. The dynamics processes started following excitation to the n_O,π^* state (S_1) can be described by four types of trajectories: (i) In 41% of all trajectories, the relaxation process on the S_1 PES shifts the molecule into minimum, where it stays trapped until the end of simulation time. (ii) In 37% of trajectories, initial relaxation leaves in the system enough energy for surmounting the excited-state energy barrier for N−CO dissociation, and the molecule moves to the region of the crossing seam **MXS1** related to the N−CO bond stretching. The **DMF** molecule decays to the ground state in an average time of 470 fs. In the ground-state PES, two separated fragments move further apart, and the energy deposited by excitation is mostly transferred to their kinetic energy. An example of this type of trajectory is shown in Figure 5. (iii) In the third type of trajectories (13% of all trajectories), molecules decay to the ground state again via **MXS1**, yielding HCO and $N(CH_3)_2$ fragments, which recombine to the ground-state **DMF** molecule. This indicates that their kinetic energy is not sufficient for realizing fast separation. (iv) In 7% of trajectories deactivated to the ground state, $N(CH_3)_2$ radical abstracts the hydrogen atom from the CHO fragment yielding $NH(CH_3)_2$ and CO as the final products. Additionally, in one of two remaining atypical trajectories, N−CH_3 dissociation on the S_1 PES is observed and in another **DMF** switches to the ground state via hopping point very close to the **MXS4** seam and undergoes the N−CO dissociation on the S_0 PES. It is interesting to note that in formamide the related MXS was involved in 7% of trajectories.[16] This is in accordance with an increase in the relative energy of this MXS upon passing from formamide to **DMF**, as predicted by static calculations. To summarize, in almost all hopping points (97% of the population that appears on the S_0), the N−CO bond in **DMF** is found to be strongly stretched (average value 2.30 Å), indicating that the N−CO dissociation process in the first excited singlet PES is the major primary deactivation channel from the S_1 state to the ground-state photoproducts. The average time for the deactivation through the **MXS1** crossing seam from the trajectories belonging to types ii, iii, and iv is calculated to be 413 fs.

On the basis of the single trajectory observed for N−CH_3 bond fission in the excited state, it is not possible to discuss mechanistic aspects of this process. It should be noted that Liu et al.[11] suggested that this process takes place in the triplet state. Given that 41% of the population in dynamics simulations did not undergo deactivation until the end of the simulation time, some of these trajectories might be candidates for intersystem crossing to the triplet state, thus opening new primary dissociation pathways. To get qualitative insight into this possibility, a search for a possible S_1/T_1 conical intersection was undertaken. This led to the location of two S_1/T_1 structures, **MXS8** and **MXS9**, both of them being higher in energy by 4.99 eV relative to the S_0. Their structures are depicted in Figure SI1 in the Supporting Information. Analysis of spin orbit matrix elements indicates that ISC process involving **MXS8** is more probable and could indeed take place.[41] Because this possibility cannot be considered with the present version of the NEWTON-X program package as yet, this possibility could not be observed in dynamic simulations.

Summarizing the results discussed so far, we conclude that results of our dynamics simulations are in accordance with the conclusion of Fang and coworkers[11] that experimentally observed dissociation products in the ground state originate from the dissociation in the S_1 state. It is instructive to compare the present results with those obtained earlier for formamide. Both molecules exhibit similar types of trajectories, but their distribution is different. This holds in particular for the percentage of trajectories that remain undissociated in the S_1 state, which is by far larger in **DMF** than in formamide (41% in **DMF** vs 15%

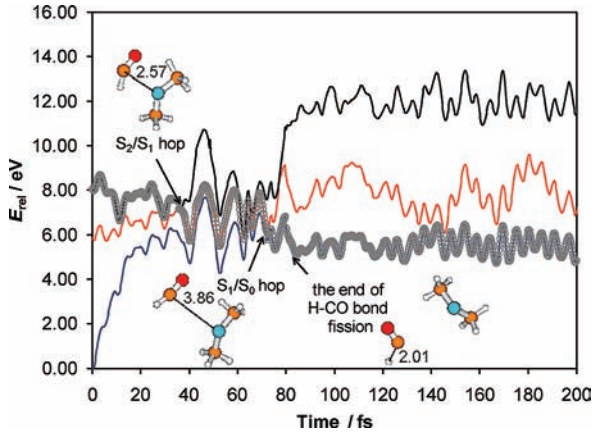

Figure 6. Time evolution of potential energies of the excited states and in the characteristic trajectory representing the N−CO stretching path with S_2 being the initial state. The dots in the potential energy graphs indicate the current state of the system.

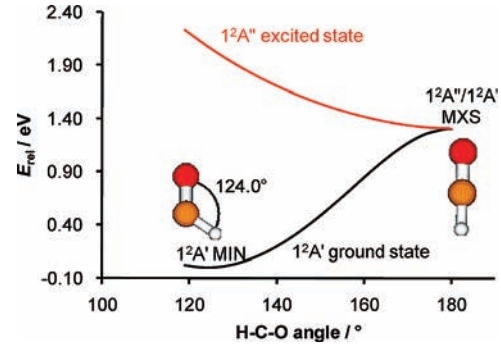

Figure 7. Ground- and the excited-state H−C−O bending reaction coordinate optimized at the CASSCF(5,4)/6-31G(d) level of theory. The energies are calculated relative to the $1^2A'$ minimum.

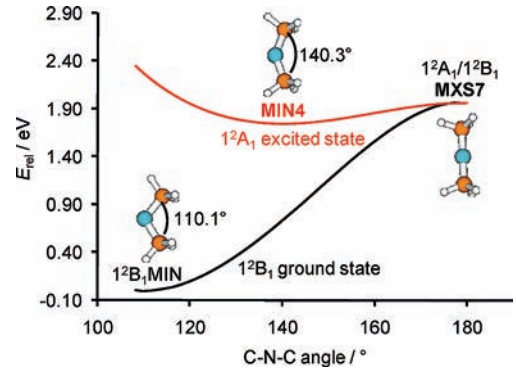

Figure 8. Ground- and the excited-state C−N−C bending reaction coordinate optimized at the CASSCF(8,7)/6-31G(d) level of theory. The energies are related to the 1^2B_1 minimum of $N(CH_3)_2$ radical.

in formamide). There is also a difference in the behavior of the NR_2 (R═H, CH_3) and HCO fragments after reaching the ground state. Specifically, the fraction of trajectories characterized by recombination into parent molecule in the ground state is larger in **DMF**, whereas abstraction of the H atom from HCO by NR_2 radical is more abundant in formamide.

D. Description of Typical Trajectories for Dissociation from the S_2 State. In the dynamics simulation following electronic excitation to the S_2 ($\pi-\pi^*$) state, initial motion in the system in all trajectories corresponds to a very fast N−CO bond stretching, which starts immediately after photoexcitation and leads to the S_2/S_1 surface crossing. The deactivation to the S_1 state is completed in an average time of only 26 fs. A similar process was observed earlier in 68% of trajectories in the parent formamide, where decay to the S_1 state took an average of 31 fs.[16] Subsequently, 82% of this type of trajectories in **DMF** decays to the S_0 state in an average time of 82 fs. A typical example of this type of trajectories is shown in Figure 6.

It is important to note that the average separation of the CHO and the $N(CH_3)_2$ fragments in the vicinity of the S_1/S_0 hopping point is about 5 Å. In other words, full N−CO dissociation gets accomplished before reaching the ground state producing electronically excited HCO and $N(CH_3)_2$ radicals. After reaching the ground state, the CHO and $N(CH_3)_2$ fragments undergo further separation in 55% of trajectories, whereas in 27% trajectories, dissociation of hydrogen atom from HCO with an average delay of 51 fs after hopping to the ground state is observed. Finally, in 18% of trajectories the molecules do not decay to the ground state until the end of the overall simulation time of 500 fs, indicating that some new mechanistic features for the S_1/S_0 quenching related to the conical intersection between the ground and the excited state in HCO or $N(CH_3)_2$ radicals might be expected. This, as discussed in detail in previous papers,[7,8,11] could proceed through two deactivation channels, leading to $HCO(\tilde{X}^2A') + N(CH_3)_2(\tilde{A}^2A_1)$ or $HCO(A^2A_1) + N(CH_3)_2(\tilde{X}^2B_1)$ products. To explore which of them prevails, a detailed search for critical points on the ground and the first excited singlet state for HCO and $N(CH_3)_2$ radicals was undertaken.

For this purpose, we first optimized the structure of HCO in the ground state ($1^2A'$) using the SA-2-CASSCF(5,4)/6-31G(d) method. In this way, the minimum energy structure with the H−C−O bending angle of 124.0° was obtained (Figure 7). Following the minimum energy pathway for this structure in the ground and the excited states along the H−C−O bending mode led to the linear HCO structure 1.31 eV above the ground-state ($1^2A'$) minimum. The energies of the ground state and excited state in this point are degenerate, and this critical point on the PES represents the maximum on the ground and minimum on the excited state PES at the same time. Therefore, we shall denote it as **MXS6**. A similar feature was recently invoked in explaining the α-CC bond breaking process in acetone on the S_1 surface.[42,43] Namely, in this case, CC bond cleavage is accompanied by π-bond formation between the two in plane p orbitals of the carbonyl group in the CCO moiety. This requires rehybridization of three sp^2 orbitals of the central carbon atom in the CCO fragment into one π and two sp orbitals, resulting in the linear structure. The results of the above analysis indicate that if the HCO radical in its excited state was formed by N−CO dissociation in **DMF**, then the relaxation process on the S_1 PES could be expected to lead directly to the vicinity of the linear conical intersection between the excited and ground states **MXS6** where the population will drain out. The system will remain on the excited state PES only as long as the relaxation process lasts. This is also in accordance with the experimental finding that HCO formed in its excited state undergoes predissociation to H + CO on a time scale of nanoseconds.[44]

Next, we applied the same approach to characterize possible critical structures for relaxation of the $N(CH_3)_2$ radical to the ground state employing the CASSCF(7,6)/6-31G(d) method. The resulting minimum-energy pathways and schematic presentation of the critical structures are shown in Figure 8. In contrast with HCO, an excited state minimum (1^2A_1 by imposing C_{2v} symmetry) with the C−N−C bending angle of 140.3° is found 1.74 eV above the ground-state minimum (1^2B_1).[45] Further opening of the C−N−C angle led to the linear structure $N(CH_3)_2$

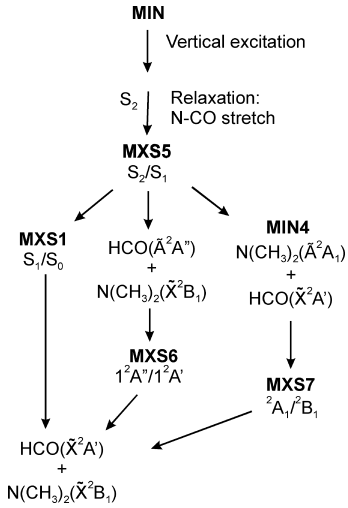

Figure 9. Schematic presentation of proposed dissociation paths following excitation to the S_2 state.

1.96 eV above the ground state (1^2B_1) minimum in which the energies of both states are degenerate (**MXS7**). Because the latter is only 0.22 eV higher than the energy of the S_1 minimum, it is reasonable to assume that deactivation of $N(CH_3)_2$ could proceed through this channel if there is enough energy in the system. However, the existence of the minimum on the path from FC to **MXS7** on the S_1 PES could slow down the deactivation process and can even keep some energy-poor population on the S_1 PES. To compare energies of so obtained CHO and $N(CH_3)_2$ radicals in the ground state and in the S_1 excited state with the energy of the starting **DMF**, optimization of the adduct $HCO\cdots N(CH_3)_2$ with the $N\cdots CO$ bond distance fixed to 10 Å (denoted as **MIN3**) is performed with the CASSCF(10,8)/6-31G(d) method. We then recalculated the relative energies of **MXS6** and **MXS7** with respect to the energy of the ground state **DMF** by adding 1.31 and 1.96 eV, respectively, to the relative energy of **MIN3** (3.58 eV, Table 1). Because the S_1 state is populated from the S_2/S_1 crossing points somewhere around the **MXS5** (5.35 eV), the **MXS6** located at the 4.87 eV is easily accessible. However, if N−CO photodissociation proceeds through the channel leading to the $HCO(\tilde{A}^2A') + N(CH_3)_2(\tilde{X}^2B_1)$ products, then it is questionable whether the **MXS7** will become activated because its energy is 0.13 eV higher than the energy of the **MXS5**. It is noteworthy that this difference increases to 0.64 and 0.73 eV at the MRCISD and MRCISD+Q computational levels, respectively.

Schematic presentation of discussed reaction paths following excitation to the S_2 state including MXSs obtained in the above analysis is displayed in Figure 9.

To gain an insight into the availability of these channels in the calculated trajectories, let us analyze geometric features of the S_1/S_0 hopping points observed in dynamics simulations following excitation to the S_2 initial excited state. The structures are divided into three groups related to the S_1/S_0 MXSs: **MXS1**, **MXS6**, and **MXS7**. Structures with H−C−O and C−N−C angles larger than 150° are associated with **MXS6** and **MXS7**, respectively. Interestingly, no structures possessing both angles larger than 150° are found. Structures with the H−C−O and C−N−C bending angles smaller than 150° and N−CO bond distance shorter than 5 Å are related to **MXS1**. The average times for evolution from the FC point to the hopping points structurally related to **MXS1**, **MXS6**, and **MXS7** are estimated to be 26, 75, and 137 fs, respectively. Somewhat surprisingly, only 10% of trajectories are found to decay through the **MXS1** that was activated in most of the trajectories when the dynamics was started from the S_1 initial state. This could be ascribed to high velocity in the N−CO direction following excitation to the S_2 initial excited state. Concomitantly, the system spends only a short time in the vicinity of **MXS1**, which is not enough for its activation. A similar effect was recently also observed in the dynamics simulations of 9*H*-adenine, where the molecule moves along a sequence of conformations with conical intersections without hopping.[46] The percentage of hopping events near **MXS6** and the **MXS7** is found to be significantly larger and comparable (33 vs 37). This would imply that the probability of channels $HCO(\tilde{X}^2A') + N(CH_3)_2(\tilde{A}^2A_1)$ and $HCO(\tilde{A}^2A') + N(CH_3)_2(\tilde{X}^2B_1)$ should be similar, which is in sharp contrast with the experimental finding that deactivation leads exclusively to $HCO(\tilde{X}^2A') + N(CH_3)_2(\tilde{A}^2A_1)$ products.

After hopping to the ground state, the energy is transferred to the translational motion of the HCO and $N(CH_3)_2$ fragments (55% of trajectories) and to additional C−H dissociation from vibrationally hot HCO fragment (27% of all trajectories). The average delay time for the C−H dissociation after S_1/S_0 hopping, calculated by applying a 2 Å limit (where 2 Å refers to the fully dissociated C−H bond), was estimated to be 51 fs. It is interesting to note that C−H dissociation occurs in trajectories that decay to the S_0 state in the vicinity of the **MXS6**.

E. Comparison with the Experimental Results. As discussed in the previous section, our dynamics calculations from the S_2 state showed that N−CO bond photodissociation leads to the formation of dissociation fragments in the ground as well as in the excited state, which is in accordance with the proposition made in experimental work of Butler and coworkers.[7,8] Furthermore, calculations predict that the formation of the ground-state products via eq 1 is fast, whereas the photodissociation channel involving the formation of $HCO(\tilde{X}^2A')$ and $N(CH_3)_2(\tilde{A}^2A_1)$ products proceeds more slowly. Given that 82% of the trajectories deactivate, the branching ratio between these two channels (82:18) is, however, in strong disagreement with the experimentally estimated branching ratio of (0.15 ± 0.04): (0.49 ± 0.09). The reason behind this discrepancy can be, at least partially, traced back to the artificially high S_2 vertical excitation energy in the FC point obtained by the CASSCF method. Consequently, the system has sufficient internal energy to activate the decay of $N(CH_3)_2(1^2A_1)$, which requires passage through the uphill **MXS7**. However, its activation under experimental conditions was less probable because of the fact that the energies of absorption band (6.42 eV) and laser (6.28 eV) used in experimental setup[8] were similar. Furthermore, there is a difference in the initial conditions between the experiment and the simulation. In the experiment, the use of high nozzle temperature (235°) was required[8] to reduce the presence of clusters in the supersonic expansion, whereas the calculations refer to the isolated molecule at 0 K without considering thermal effects. Furthermore, very fast H−C dissociation that follows after the HCO relaxes to the ground state PES could not be observed experimentally because of high background counts in detector.

Conclusions

The photodissociation of *N*,*N*-dimethylformamide in its low-lying singlet excited n_O,π^* and π,π^* states has been explored by the ab initio calculations direct trajectory surface-hopping method based at the state average CASSCF(10,8)/6-31G(d) level. Stationary points (energy minima and saddle points) and minima on the crossing seam have been located for the singlet energy surfaces of the considered singlet excited states. Com-

parison with the previously published results for formamide reveals that the replacement of the amino hydrogen atoms with the methyl groups leads to pronounced lengthening of the lifetime in the S_1 excited state (by almost 700 fs), whereas deactivation process in the S_2 state proceeds much faster. The dynamics simulations starting in the first excited singlet state (n_O,π^*) showed that in 57% of trajectories, S_1 excited **DMF** decays to the ground state via the crossing seam **MXS1** related to N−CO bond stretching. In 41% of all trajectories, the relaxation process on the S_1 PES moves the molecule into minimum, where it stays trapped until the end of simulation time. In simulations starting in the second excited state, all of trajectories are found to deactivate through **MXS5** (S_2/S_1) by very fast N−CO stretching. However, the largest portion of the population overshoots the **MXS1** because the N−CO dissociation proceeds very fast in the S_2 state and continues in the S_1, leading to fully dissociated electronically excited HCO and $N(CH_3)_2$ radicals. In other words, full N−CO dissociation gets accomplished before the ground state is reached. On the basis of the detailed search of critical points on the ground and the first excited state for HCO and $N(CH_3)_2$ radicals, a possible mechanism for the decay of the HCO($1^2A''$) and $N(CH_3)_2$(1^2A_1) radicals to the ground state was proposed. The decay of the HCO($1^2A''$) species takes place through the **MXS6**, which is lower in energy than the S_2/S_1 MXS (**MXS5**); consequently, it is easily accessible. However, deactivation of $N(CH_3)_2$(1^2A_1) requires passage through the uphill **MXS7**, and its decay to the ground state is less probable unless there is enough energy in the system to overcome the barrier.

Acknowledgment. We acknowledge support by the Ministry of Science, Education and Sport of Croatia through the project 098-0982933-2920 and the WTZ treaty between Austria and Croatia (project no. HR17/2008). The support by the COST D37 action, WG0001-06, is also acknowledged. The calculations were partially performed on the Schroedinger III Linux cluster of the Vienna University Computer Centre.

Supporting Information Available: Key structural parameters of the structures of the singlet/triplet **MXS8** and **MXS9** of **DMF** calculated at CASSCF(10,8)/6-31G(d) level of theory and total electronic energies (au) and Cartesian coordinates (angstroms) of *N*,*N*-dimethylformamide, saddle points, and minima on the crossing seam calculated by the SA-3-CASSCF(10,8)/6-31G(d) and MR-CISD[8,6]/6-31G(d) methods. This material is available free of charge via the Internet at http://pubs.acs.org.

References and Notes

(1) (a) Challender, R. H.; Dyer, R. B.; Gilmanshin, R.; Woodruff, W. H. *Annu. Rev. Phys. Chem.* **1998**, *49*, 173. (b) Cheng, Q.; Steinmetz, M. G.; Jayaraman, V. *J. Am. Chem. Soc.* **2002**, *124*, 7676. (c) Wang, Y.; Hu, X. *J. Am. Chem. Soc.* **2002**, *124*, 8445.

(2) For example: Sionkowska, A. *J. Photochem. Photobiol., A* **2006**, *117*, 61–67, and references cited therein.

(3) Hildebrandt, P.; Tsuboi, M.; Soiro, T. G. *J. Phys. Chem. A* **1990**, *94*, 2274.

(4) Lundell, J.; Krajewska, M.; Räsänen, M. *J. Phys. Chem. A* **1998**, *102*, 6643.

(5) Bosoco, S.; Cirllo, A.; Timmons, R. B. *J. Am. Chem. Soc.* **1969**, *9*, 3140.

(6) (a) Mayne, L. C.; Hudson, B. S. *J. Phys. Chem.* **1991**, *95*, 2962. (b) Markham, L. M.; Hudson, B. S. *J. Phys. Chem.* **1996**, *100*, 2731.

(7) Forde, N. R.; Myers, T. L.; Butler, L. J. *Faraday Discuss.* **1997**, *108*, 221–242.

(8) Forde, N. R.; Butler, L. J.; Abrash, S. A. *J. Chem. Phys.* **1999**, *110*, 8954.

(9) Pei, K.-M.; Ma, Y.; Zheng, X. *J. Chem. Phys.* **2008**, *128*, 224310.

(10) Liu, D.; Fang, W.-H.; Fu, X.-Y. *Chem. Phys. Lett.* **2000**, *318*, 291.

(11) Liu, D.; Fang, W. H.; Lin, Z. Y.; Fu, X. Y. *J. Chem. Phys.* **2002**, *117*, 9241.

(12) (a) Antol, I.; Eckert-Maksić, M.; Lischka, H. *J. Phys. Chem. A* **2004**, *108*, 10317. (b) Antol, I.; Barbatti, M.; Eckert-Maksić, M.; Lischka, H. *Monatsh. Chem.* **2008**, *139*, 319.

(13) Chen, X.-B.; Fang, W.-H.; Fang, D. C. *J. Am. Chem. Soc.* **2003**, *125*, 9689.

(14) Petersen, Ch.; Dahl, N. H.; Jensen, S. K.; Thgersen, J.; Keiding, S. R. *J. Phys. Chem. A* **2008**, *112*, 3339, and references cited therein.

(15) (a) Boden, J. C.; Back, R. A. *Trans. Faraday. Soc.* **1970**, *66*, 175. (b) Back, R. A.; Boden, J. C. *Trans. Faraday. Soc.* **1971**, *69*, 88.

(16) Antol, I.; Eckert-Maksić, M.; Barbatti, M.; Lischka, H. *J. Chem. Phys.* **2007**, *127*, 234303.

(17) Antol, I.; Vazdar, M.; Barbatti, M.; Eckert-Maksić, M. *Chem. Phys.* **2008**, *349*, 308.

(18) Barbatti, M.; Granucci, G.; Persico, M.; Ruckenbauer, M.; Vazdar, M.; Eckert-Maksić, M.; Lischka, H. *J. Photochem. Photobiol., A* **2007**, *190*, 228.

(19) Shepard, R.; Lischka, H.; Szalay, P. G.; Kovar, T.; Ernzerhof, M. *J. Chem. Phys.* **1992**, *96*, 2085.

(20) Shepard, R. In *Modern Electronic Structure Theory, Part I*; Yarkony, D. R., Ed.; World Scientific: Singapore, 1995; p 345.

(21) Lischka, H.; Dallos, M.; Shepard, R. *Mol. Phys.* **2002**, *100*, 1647.

(22) Lischka, H.; Dallos, M.; Szalay, P. G.; Yarkony, D. R.; Shepard, R. *J. Chem. Phys.* **2004**, *120*, 7322.

(23) Dallos, M.; Lischka, H.; Shepard, R.; Yarkony, D. R.; Szalay, P. G. *J. Chem. Phys.* **2004**, *120*, 7330.

(24) (a) Barbatti, M.; Ruckenbauer, M.; Lischka, H. *J. Chem. Phys.* **2005**, *122*, 174307. (b) Barbatti, M.; Vazdar, M.; Aquino, A. J. A.; Eckert-Maksić, M.; Lischka, H. *J. Chem. Phys.* **2006**, *125*, 164323. (c) Barbatti, M.; Pittner, J.; Lischka, H. *Chem. Phys.* **2009**, *356*, 147. (d) Szymczak, J. J.; Barbatti, M.; Lischka, H. *J. Chem. Theor. Comp.* **2008**, *4*, 1189–1199.

(25) Tully, J. C. *J. Chem. Phys.* **1990**, *93*, 1061.

(26) Hammes-Schiffer, S.; Tully, J. C. *J. Chem. Phys.* **1994**, *101*, 4657.

(27) Swope, W. C.; Andersen, H. C.; Berens, P. H.; Wilson, K. R. *J. Chem. Phys.* **1982**, *76*, 37.

(28) Wigner, E. *Phys. Rev.* **1932**, *40*, 749.

(29) Lischka, H.; Shepard, R.; Shavitt, I.; Pitzer, R. M.; Dallos, M.; Müller, Th.; Szalay, P. G.; Brown, F. B.; Ahlrichs, R.; Böhm, H. J.; Chang, A.; Comeau, D. C.; Gdanitz, R.; Dachsel, H.; Ehrhardt, C.; Ernzerhof, M.; Höchtl, P.; Irle, S.; Kedziora, G.; Kovar, T.; Parasuk, V.; Pepper, M. J. M.; Scharf, P., Schiffer, H.; Schindler, M.; Schüler, M.; Seth, M.; Stahlberg, E. A.; Zhao, J.-G.; Yabushita, S.; Zhang, Z.; Barbatti, M.; Matsika, S.; Schuurmann, M.; Yarkony, D. R.; Brozell, S. R.; Beck, E. V.; Blaudeau, J.-P. *COLUMBUS*, an ab initio electronic structure program, release 5.9.1, 2006. www.univie.ac.at/columbus.

(30) Helgaker, T.; Jensen, H. J. Aa.; Jørgensen, P.; Olsen, J.; Ruud, K.; Aigren, H.; Andersen, T.; Bak, K. L.; Bakken, V.; Christiansen, O.; Dahle, P.; Dalskov, E. K.; Enevoldsen, T.; Heiberg, H.; Hettema, H.; Jonsson, D.; Kirpekar, S.; Kobayashi, R.; Koch, H.; Mikkelsen, K. V.; Norman, P.; Packer, M. J.; Saue, T.; Taylor, P. R.; Vahtras, O. *DALTON*, an ab initio electronic structure program, release 1.0, 1997.

(31) Becke, A. D. *J. Chem. Phys.* **1993**, *98*, 5648.

(32) Schäfer, A.; Horn, H.; Ahlrics, R. *J. Chem. Phys.* **1992**, *97*, 2571.

(33) Ahlrics, A.; Bär, M.; Häser, M.; Horn, H.; Kölmel, C. *Chem. Phys. Lett.* **1989**, *162*, 165.

(34) (a) Hehre, W. J.; Ditchfield, R.; Pople, J. A. *J. Chem. Phys.* **1972**, *56*, 2257. (b) Hariharan, P. C.; Pople, J. A. *Theor. Chim. Acta* **1973**, *28*, 213.

(35) Barbatti, M.; Granucci, G.; Ruckenbauer, M.; Persico, M.; Lischka, H. *NEWTON-X*, a package for Newtonian dynamics closing to the crossing seam, version 0.14a, 2007. www.univie.ac.at/newtonx.

(36) Hunt, H. D.; Simpson, W. T. *J. Am. Chem. Soc.* **1953**, *75*, 4540.

(37) Kaya, K.; Nagakura, S. *Theor. Chim. Acta* **1967**, *7*, 117.

(38) Serrano-Andrés, L.; Fülscher, M. P. *J. Am. Chem. Soc.* **1996**, *118*, 12190.

(39) Li, Y.; Garrell, R. L.; Houk, K. N. *J. Am. Chem. Soc.* **1991**, *113*, 5895.

(40) Langhoff, S. R.; Davidson, E. R. *Int. J. Quantum Chem.* **1974**, *8*, 61.

(41) Spin-orbit matrix elements were calculated using CASSCF(10,8)/6-31G(d) method with the MOLPRO program package. For the **MXS8**, the following values were obtained:−19.97i cm^{-1} (X), 37.12 cm^{-1} (Y), and−6.64i cm^{-1} (Z). The corresponding values for the **MXS9** amount - 0.69i cm^{-1} (X), 0.29 cm^{-1} (Y), and −0.65i cm^{-1} (Z).

(42) Diau, E. W.-G.; Kötting, C.; Zewail, A. H. *ChemPhysChem* **2001**, *2*, 273.

(43) Antol, I.; Eckert-Maksić, M.; Ončák, M.; Slaviček, P.; Lischka, H. *Collect. Czech. Chem. Commun.* **2008**, *73*, 1475.

(44) (a) Vadusev, R.; Zare, R. N. *J. Chem. Phys.* **1982**, *76*, 5267. (b) Stone, B. M.; Noble, M.; Lee, E. K. C. *Chem. Phys. Lett.* **1985**, *118*, 83. (c) Chuang, M.-C.; Foltz, M. F.; Moore, C. B. *J. Chem. Phys.* **1987**, *87*, 3855. (d) Wagner, A. F.; Bowman, J. M. *J. Phys. Chem.* **1987**, *91*, 5314.

(e) Timonen, R. B.; Ratjczak, E.; Gutman, D.; Wagner, A. F. *J. Phys. Chem.* **1987**, *91*, 5325.

(45) In this context, we should mention that the minimum energy structure for $N(CH_3)_2$ in the excited state calculated using CIS approach was previously reported by Butler and coworkers.[7,8] Our results are in qualitative agreement with their finding. Therefore, in our calculations, the excited state (1^2A_1 by imposing C_{2v} symmetry) structure was found to lie 1.74 eV above the ground-state (1^2B_1) minimum (Figure 8), which is ca. 0.2 eV greater than that reported by Butler.[8] The main geometrical features of the calculated structures are also similar. In particular, both 1^2A_1 structures are characterized by widely opened C−N−C bending angle, which in the framework of CASSCF calculations is 143.3°, as compared with 145° obtained at the CIS level. The corresponding angles in the ground state are 110.1 and 110.6°, respectively.

(46) Barbatti, M.; Lischka, H. *J. Am. Chem. Soc.* **2008**, *130*, 6831.

JP9046177